M-Estimation-Based Minimum Error Entropy with Affine Projection Algorithm for Outlier Suppression in Spaceborne SAR System

*WANG Weixin, CHANG Xuelian, OU Shifeng**

College of Physics and Electronic Information, Yantai University, Yantai 264005, P. R. China

(Received 9 July 2025; revised 8 August 2025; accepted 15 August 2025)

Abstract: Conventional adaptive filtering algorithms often exhibit performance degradation when processing multipath interference in raw echoes of spaceborne synthetic aperture radar (SAR) systems due to anomalous outliers, manifesting as insufficient convergence and low estimation accuracy. To address this issue, this study proposes a novel robust adaptive filtering algorithm, namely the M-estimation-based minimum error entropy with affine projection (APMMEE) algorithm. This algorithm inherits the joint multi-data-block update mechanism of the affine projection algorithm, enabling rapid adaptation to the dynamic characteristics of raw echoes and achieving fast convergence. Meanwhile, it incorporates the M-estimation-based minimum error entropy (MMEE) criterion, which weights error samples in raw echoes through M-estimation functions, effectively suppressing outlier interference during the algorithm update. Both the system identification simulations and practical multipath interference suppression experiments using raw echoes demonstrate that the proposed APMMEE algorithm exhibits superior filtering performance.

Key words: radar signal; adaptive filtering; minimum error entropy; M-estimation; affine projection

CLC number: V243 **Document code:** A **Article ID:** 1005-1120(2025)05-0615-14

0 Introduction

Spaceborne synthetic aperture radar (SAR) is an active microwave remote sensing system onboard satellites that achieves high-resolution imaging through synthetic aperture and pulse compression techniques. Its all-weather and day-night operational capabilities make it essential for the Earth observation and disaster monitoring[1]. The imaging quality depends fundamentally on echo signal purity, with multipath effects in complex scenes being a primary limiting factor. Multipath phenomena in spaceborne SAR exhibit dual characteristics: Constructive multipath (e.g., building double reflections or slope-directed scattering) provides target 3D information to supplement terrain analysis, whereas redundant interference from urban canyons or sea waves degrades the signal integrity and requires suppression[2]. This study focuses on the latter case—detrimental redundant multipath interference that induces ghost targets and edge blurring in SAR imagery[3]. Precise suppression of multipath-induced outliers at the raw echo stage is therefore critical for enhancing the SAR performance.

Conventional approaches like constant false alarm rate detection[4] and digital beamforming[5] show limitations in dynamic environments. Adaptive filtering algorithms overcome these constraints by dynamically tracking interference without requiring signal stationarity assumptions. The least mean square (LMS) algorithm[6-7] offers low computational complexity but suffers from slow convergence. While the recursive least squares (RLS)[8-9] im-

*Corresponding author, E-mail address: ousfeng@ytu.edu.cn.

How to cite this article: WANG Weixin, CHANG Xuelian, OU Shifeng. M-estimation-based minimum error entropy with affine projection algorithm for outlier suppression in spaceborne SAR system[J]. Transactions of Nanjing University of Aeronautics and Astronautics, 2025,42(5):615-628.

http://dx.doi.org/10.16356/j.1005-1120.2025.05.005

proves the convergence, it increases computational costs and exhibits the instability. Affine projection (AP) algorithms[10-11] enhance the stability but remain sensitive to outliers.

Recent advances in information-theoretic learning (ITL)[12-14] highlight the minimum error entropy (MEE) criterion, which excels in capturing higher-order signal statistics and performs robustly in non-Gaussian noise[15-16]. The affine projection minimum error entropy (APMEE) algorithm[17] combines AP's fast convergence with MEE's impulse noise resistance. However, MEE using quadratic Rényi entropy[18-19] underperforms with heavy-tailed/multimodal noise, where extreme outliers distort the error analysis[20-22]. The M-estimation-based MEE (MMEE) criterion[23-25] suppresses outliers via error weighting, enhancing the robustness in non-Gaussian environments, yet fails to co-optimize the convergence speed and steady-state accuracy.

To address these challenges, we propose a novel robust adaptive filtering algorithm which is M-estimation-based MEE with AP (APMMEE). Its core innovation lies in the organic integration of the fast convergence characteristics of AP algorithm with the strong robustness of MMEE criterion. Theoretical analysis reveals intrinsic consistency between the sliding window length in MMEE criterion and the subspace dimension in the AP algorithm. Based on reproducing kernel Hilbert space (RKHS)[26-27] theory, Gaussian kernel[28] transforms the total error minimization problem into an adaptively solvable optimization model. Inheriting AP's multi-data-block joint updating mechanism, it achieves rapid convergence, Simultaneously, the MMEE criterion employs M-estimation to weight error samples based on posterior error magnitude, effectively suppressing outlier interference and significantly enhancing impulsive noise resistance. Comparative experiments and processing tests with actual spaceborne SAR echo data demonstrate that the APMMEE algorithm effectively overcomes the technical challenge of traditional algorithms' sensitivity to outliers in non-stationary multipath environments. The algorithm exhibits superior filtering performance in complex noise environments, making it particularly suitable for preprocessing raw echo data in spaceborne SAR systems. By precisely suppressing anomalous outliers caused by redundant multipath interference, it achieves signal purification prior to critical imaging steps such as range compression and azimuth focusing, thereby fundamentally reducing interference effects on subsequent imaging quality and establishing a stable, reliable data foundation for high-resolution SAR imaging.

1 Overview of Existing Related Algorithms

1.1 Algorithmic model

In typical complex multipath propagation environments of radar systems, establishing accurate signal models forms the foundation for multipath interference suppression research. For spaceborne SAR echo characteristics, the radar transmits baseband pulse signals $\boldsymbol{s}(n)$ using linear frequency modulated (LFM) waveforms[29], which are standard in SAR systems. As the core waveform for spaceborne SAR imaging, LFM signals achieve large bandwidth through linear variation of instantaneous frequency during the pulse duration, enabling pulse compression via frequency modulation. The signal parameters of carrier frequency f_0=5.4 GHz and bandwidth B=200 MHz are selected to match practical engineering scenarios while enhancing model specificity.

Physically, spaceborne SAR raw echoes fundamentally represent the convolution of transmitted signals with ground scattering functions. When incorporating multipath effects, the $\boldsymbol{r}_m(n)$[30] model becomes

$$\boldsymbol{r}_m(n)=\boldsymbol{s}(n)*\sigma(n)+\sum_{k=1}^{K}\alpha_k\cdot\boldsymbol{s}(n-\tau_k)*\sigma_k(n)+\boldsymbol{v}(n) \tag{1}$$

where "*" denotes the convolution operation, and $\boldsymbol{s}(n)$ the transmitted LFM signal. The first term of $\boldsymbol{s}(n)*\sigma(n)$ corresponds to the direct-path echo, containing the true target scattering information to be

preserved, where $\sigma(n)$ is the complex reflection function of ground targets. The second term represents redundant multipath interference. Here K is the number of multipaths; α_k the attenuation coefficient of the kth path characterizing signal energy loss during the propagation; τ_k the crucial time delay (differential between multipath and direct signals), serving as the key feature of multipath phenomena in the convolution model; $\sigma_k(n)$ the reflection function of corresponding scatterers, which constitutes the suppression target of the algorithm, and $\boldsymbol{v}(n)$ additive noise comprising thermal noise and environmental clutter.

To adapt to the adaptive filtering framework, the desired received signal is redefined as

$$\boldsymbol{d}(n)=\boldsymbol{y}(n)+\boldsymbol{v}(n)=\sum_{k=1}^{K}\alpha_k\cdot\boldsymbol{x}^{\mathrm{T}}(n-\tau_k)*\boldsymbol{w}_0+\boldsymbol{v}(n) \tag{2}$$

where $\boldsymbol{y}(n)$ denotes the redundant multipath interference component, $\boldsymbol{x}(n)$ the reference input for correlation computation, $\boldsymbol{w}_0$ the weight vector of the target system, and $\boldsymbol{v}(n)$ zero-mean Gaussian white noise with variance σ_v^2.

The system error at the nth iteration, $\boldsymbol{e}(n)$, is defined as

$$\boldsymbol{e}(n)=\boldsymbol{d}(n)-\sum_{k=1}^{K}\alpha_k\cdot\boldsymbol{x}^{\mathrm{T}}(n-\tau_k)*\boldsymbol{w}(n)+\boldsymbol{v}(n) \tag{3}$$

where $\boldsymbol{w}(n)$ represents the current weight vector. The adaptive filtering technique dynamically optimizes $\boldsymbol{w}(n)$ to asymptotically converge to the target weight vector $\boldsymbol{w}_0$, thereby establishing the theoretical foundation for precise suppression of redundant multipath interference in spaceborne SAR raw echoes.

1.2 Review of AP algorithm

Compared with the conventional LMS algorithm, the AP algorithm significantly improves the convergence speed by constructing an affine projection input matrix utilizing multiple input vectors. Here, the input signal matrix is $\boldsymbol{X}(n)=[\boldsymbol{x}(n),\boldsymbol{x}(n-1),\cdots,\boldsymbol{x}(n-P+1)]$, with dimensions of $k\times P$. In this context, P denotes the projection order of the AP algorithm, and k the filter length. The algorithm can be described by the following constrained optimization rule

$$\min_{\boldsymbol{w}(n+1)}\|\boldsymbol{w}(n+1)-\boldsymbol{w}(n)\|_2^2$$
$$\text{s.t. }\boldsymbol{d}(n)-\boldsymbol{X}^{\mathrm{T}}(n)\boldsymbol{w}(n+1)=0 \tag{4}$$

where $\|\cdot\|_2$ denotes the l_2 norm, and the desired signal is $\boldsymbol{d}(n)=[\boldsymbol{d}(n),\boldsymbol{d}(n-1),\cdots,\boldsymbol{d}(n-P+1)]^{\mathrm{T}}$. Based on this, the recursive formula of the AP algorithm is as follows

$$\boldsymbol{w}(n+1)=\boldsymbol{w}(n)+\mu\boldsymbol{X}(n)[\boldsymbol{X}^{\mathrm{T}}(n)\boldsymbol{X}(n)]^{-1}\boldsymbol{e}(n) \tag{5}$$

where $\boldsymbol{e}(n)=[\boldsymbol{e}(n),\boldsymbol{e}(n-1),\cdots,\boldsymbol{e}(n-P+1)]^{\mathrm{T}}$ is the error signal, and μ the step size of the algorithm. The algorithm achieves rapid convergence in Gaussian environments. However, due to the lack of an effective outlier identification mechanism and robust handling for data anomalies, the algorithm struggles to maintain stable performance when processing abnormal outliers in non-Gaussian environments, exhibiting significant drawbacks.

1.3 Review of the MMEE

The MMEE assigns lower weights to abnormal outliers through the robust weighting mechanism of M-estimation, while its integration with the minimum error entropy criterion—adaptable to data probability distribution characteristics—effectively suppresses outlier interference. M-estimation, the core methodology of robust statistics introduced by Huber, is alternatively termed maximum likelihood-type estimation due to its structural resemblance to maximum likelihood estimation. It suppresses outliers through differential weighting, assigning lower weights to samples with larger deviations and higher weights to those with smaller deviations. The optimization objective function of M-estimation is mathematically formulated as

$$\hat{w}_M=\arg\min_{\boldsymbol{w}}\sum_{i=1}^{N}\rho\left(\frac{\boldsymbol{d}_i-\boldsymbol{w}^{\mathrm{T}}\boldsymbol{x}_i}{\hat{\sigma}_i}\right) \tag{6}$$

where N represents the total number of data samples; $\rho(\cdot)$ the error loss function; $\boldsymbol{d}_i$ the desired output; $\boldsymbol{w}$ the weight vector, and $\boldsymbol{x}_i$ the input vector. $r_i=(\boldsymbol{d}_i-\boldsymbol{w}^{\mathrm{T}}\boldsymbol{x}_i)/\hat{\sigma}_i$ represents the standardized residual, and $\hat{\sigma}_i$ is typically calculated via the median

absolute deviation (MAD)

$$\hat{\sigma}_i = \frac{\text{MAD}}{0.674\,5} = \frac{\text{med}(\boldsymbol{e}_i - \text{med}(\boldsymbol{e}))}{0.674\,5} \tag{7}$$

where med (·) denotes the median operator, and 0.674 5 is the constant correction factor.

Taking the partial derivative of the objective function yields

$$\sum_{i=1}^{N} \psi(r_i)\boldsymbol{x}_i = 0 \tag{8}$$

where $\psi(\cdot) = \rho'(\cdot)$ is the score function. The weight function $\varphi(\cdot)$ can be derived from $\psi(\cdot)$: $\varphi(\cdot) = \psi(r_i)/r_i$.

For non-Gaussian noise scenarios, the Hampel weight function demonstrates outstanding performance through residual-tiered processing, defined as

$$\varphi_{\text{Hampel}}(\cdot) = \begin{cases} 1 & |r_i| \leqslant \Delta_1 \\ \dfrac{\Delta_1}{|r_i|} & \Delta_1 < |r_i| \leqslant \Delta_2 \\ \dfrac{\Delta_1}{|r_i|} \times \left(\dfrac{\Delta_3 - |r_i|}{\Delta_3 - \Delta_2} \right) & \Delta_2 < |r_i| \leqslant \Delta_3 \\ 0 & |r_i| > \Delta_3 \end{cases} \tag{9}$$

where Δ_1, Δ_2, Δ_3 are the threshold parameters of Hampel's weight function.

The MMEE method extends M-estimation by integrating its outlier-sensitive weight function $\varphi(\cdot)$ into conventional Bagger-window density estimators. By adaptively weighting or discarding error samples $\boldsymbol{e}_i$, a novel PDF kernel density estimator is constructed as

$$\hat{p}_M(x) = \frac{1}{L} \sum_{i=n-L+1}^{n} \kappa_\sigma(x - \varphi_\tau(\boldsymbol{e}_i)\cdot\boldsymbol{e}_i) \tag{10}$$

where $\varphi_\tau(\boldsymbol{e}_i)$ is the M-estimation weight factor that adjusts contributions based on sample outlier severity, L the length of the sliding window, and $\kappa_\sigma(\cdot)$ the kernel function with kernel width σ controlling smoothness, defined mathematically as

$$\kappa_\sigma(\boldsymbol{x}) = \frac{1}{\sigma\sqrt{2\pi}} \exp\left(-\frac{\boldsymbol{x}^2}{2\sigma^2} \right) \tag{11}$$

Building upon this estimator, the modified quadratic information potential (MQIP) is introduced as the cost function for MMEE entropy criteria

$$\hat{V}_2^M(\tau) = \frac{1}{L^2} \sum_{i=n-L+1}^{n} \sum_{j=n-L+1}^{n} \kappa_\sigma(\varphi_\tau(\boldsymbol{e}_i)\cdot\boldsymbol{e}_i - \varphi_\tau(\boldsymbol{e}_j)\cdot\boldsymbol{e}_j) \tag{12}$$

By maximizing the MQIP, the optimization problem for the MMEE criterion can be formulated as

$$J_{\text{MMEE}}(\boldsymbol{w}_n) = \max_{\boldsymbol{w}} \frac{1}{L^2} \sum_{i=n-L+1}^{n} \sum_{j=n-L+1}^{n} \kappa_\sigma(\varphi_\tau(\boldsymbol{e}_i)\cdot\boldsymbol{e}_i - \varphi_\tau(\boldsymbol{e}_j)\cdot\boldsymbol{e}_j) \tag{13}$$

where e_i, e_j denote the posterior errors. The robustness is enhanced through this cost function.

2 The Proposed APMMEE algorithm

Although the MMEE criterion demonstrates excellent performance in suppressing abnormal outliers through its robust weighting mechanism and adaptability to non-Gaussian distributions, its sensitive dependence on kernel function parameters, high computational complexity from higher-order statistics, and performance fluctuations under low SNR or unknown data distribution scenarios impose limitations in applications requiring both real-time operation and dynamic adaptability (e.g., adaptive filtering tasks with complex multipath interference). Notably, the AP algorithm's dynamic tracking capability through multi-step projection updates and its utilization of input correlation characteristics offer potential to compensate for these limitations. Within this research framework, we reformulate the optimization problem in Eq.(4) using the MMEE criterion. The core optimization objective is to solve for the optimal weight vector $\boldsymbol{w}$ under the norm constraint of weight updating, formally expressed as

$$\begin{aligned} &\max_{\boldsymbol{w}(t)} \frac{1}{L^2} \sum_{i=1}^{L} \sum_{j=1}^{L} \kappa_\sigma(\varphi_{e_i}(\boldsymbol{e}_p(t-i))\cdot\boldsymbol{e}_p(t-i) - \\ &\qquad \varphi_{e_j}(\boldsymbol{e}_p(t-j))\cdot\boldsymbol{e}_p(t-j)) \\ &\text{subject to } \|\boldsymbol{w}(t) - \boldsymbol{w}(t-1)\|_2^2 \leqslant \mu^2 \end{aligned} \tag{14}$$

where $\boldsymbol{w}$ denotes the weight vector, φ_e the weighting function, L the sliding window length, and σ the kernel width of the Gaussian kernel function; $\boldsymbol{e}_p(t-i)$ and $\boldsymbol{e}_p(t-j)$ indicate the posterior errors at time steps $t-i$ and $t-j$, respectively. In Eq.(14), the objective function employs adaptive weighting to dy-

namically adjust error samples, effectively mitigating outlier-induced perturbations in algorithmic updates. This mechanism drives the system toward optimizing the error distribution toward an ideal configuration, thereby enhancing overall performance. The constraint $\|\boldsymbol{w}(t)-\boldsymbol{w}(t-1)\|_2^2 \leqslant \mu^2$ rigorously bounds the variation magnitude of weight vectors between consecutive iterations. The parameter μ, governing the step size of weight updates, critically determines the system stability and convergence properties. Excessive μ values may cause aggressive weight updates, resulting in the system instability or even divergence; whereas insufficient μ values lead to prohibitively slow updates, severely degrading the convergence speed and compromising real-time applicability.

To solve this constrained optimization problem, we implement the classical Lagrange multiplier method. By introducing the Lagrange multiplier γ, the constrained problem is transformed into an unconstrained extremum problem, yielding the derived cost function as

$$J_{\text{APMMEE}}=\frac{1}{L^2}\sum_{i=1}^{L}\sum_{j=1}^{L}\kappa_\sigma(\varphi_{e_i}(e_p(t-i))\cdot\boldsymbol{e}_p(t-i)-\varphi_{e_j}(\boldsymbol{e}_p(t-j))\cdot\boldsymbol{e}_p(t-j))-\gamma[\|\boldsymbol{w}(t)-\boldsymbol{w}(t-1)\|_2^2-\mu^2] \tag{15}$$

where γ denotes the Lagrange multiplier. It functions as a balancer in this well-designed cost function to precisely regulate the relationship between the objective function and constraints. The value of γ is not arbitrarily assigned, but directly governs the optimization outcome. Larger γ values significantly increase the weight of constraints during the optimization, enforcing stricter bounds on weight updates to ensure system stability; whereas smaller γ values prioritize the objective function's optimization, driving the system toward extremum seeking for enhanced performance.

We subsequently investigate the update mechanism for weight vector $\boldsymbol{w}(t)$ by deriving the gradient of Lagrangian J_{APMMEE} with respect to $\boldsymbol{w}(t)$, which determines both the direction and magnitude of weight updates. The gradient expression is formally defined as

$$\nabla J_{\text{APMMEE}}(\boldsymbol{w}(t))=\frac{\partial J_{\text{APMMEE}}(\boldsymbol{w}(t))}{\partial \boldsymbol{w}(t)}=\frac{1}{L^2\sigma^2}\sum_{i=t-L+1}^{t}\sum_{j=t-L+1}^{t}[(\boldsymbol{u}(t-i)\varphi_{e_i}(\boldsymbol{e}_p(t-i))-\boldsymbol{u}(t-j)\varphi_{e_j}(\boldsymbol{e}_p(t-j)))\times\kappa_\sigma(\varphi_{e_i}(\boldsymbol{e}_p(t-i))\cdot\boldsymbol{e}_p(t-i)-\varphi_{e_j}(\boldsymbol{e}_p(t-j))\cdot\boldsymbol{e}_p(t-j))\times(\varphi_{e_i}(\boldsymbol{e}_p(t-i))\cdot\boldsymbol{e}_p(t-i)-\varphi_{e_j}(\boldsymbol{e}_p(t-j))\cdot\boldsymbol{e}_p(t-j))]-2\gamma[\boldsymbol{w}(t)-\boldsymbol{w}(t-1)] \tag{16}$$

where t denotes time; $\boldsymbol{u}(t-i)$ and $\boldsymbol{u}(t-j)$ represent the input vectors at time steps i and j, respectively.

This gradient formulation transcends mere mathematical manipulation, incorporating the synergistic effects of input signals, error terms, and kernel functions to establish a rigorous theoretical foundation for weight vector updates. To enhance practical utility for computational implementation and analysis, we employ mathematical simplification techniques to derive a condensed matrix-form iteration formula. To enhance notational simplicity and improve both readability and computational efficiency of the formulae, we introduce the following definitions: $\lambda_i=\varphi_{e_i}(\boldsymbol{e}_p(t-i))$, $\lambda_j=\varphi_{e_j}(\boldsymbol{e}_p(t-j))$ and $\kappa_{\sigma ij}=\kappa_\sigma(\lambda_i\boldsymbol{e}_p(t-i)-\lambda_j\boldsymbol{e}_p(t-j))$. The simplification process leverages matrix operation properties and relevant mathematical theorems. The gradient expression of the cost function obtained through rigorous derivation is as follows.

$$\begin{aligned}\nabla J_{\text{APMMEE}}(\boldsymbol{w}(t))=&\frac{1}{L^2\sigma^2}\sum_{i=t-L+1}^{t}\sum_{j=t-L+1}^{t}[(\boldsymbol{u}(t-i)\lambda_i-\boldsymbol{u}(t-j)\lambda_j)\kappa_{\sigma ij}(\lambda_i\boldsymbol{e}_p(t-i)-\lambda_j\boldsymbol{e}_p(t-j))]-2\gamma[\boldsymbol{w}(t)-\boldsymbol{w}(t-1)]=\\&\Omega_1-\Omega_2-\Omega_3+\Omega_4-2\gamma[\boldsymbol{w}(t)-\boldsymbol{w}(t-1)]=\\&2\Omega_1-2\Omega_2-2\gamma[\boldsymbol{w}(t)-\boldsymbol{w}(t-1)]=\\&\frac{2}{L^2\sigma^2}\boldsymbol{X}(t)(\boldsymbol{B}(t)-\boldsymbol{A}(t))\boldsymbol{E}_p(t)-2\gamma[\boldsymbol{w}(t)-\boldsymbol{w}(t-1)]\end{aligned} \tag{17}$$

where

$$\begin{cases}\Omega_1=\dfrac{1}{L^2\sigma^2}\displaystyle\sum_{i=t-L+1}^{t}\sum_{j=t-L+1}^{t}\boldsymbol{u}(t-i)\lambda_i\kappa_{\sigma ij}\boldsymbol{e}_p(t-i)\\ \Omega_2=\dfrac{1}{L^2\sigma^2}\displaystyle\sum_{i=t-L+1}^{t}\sum_{j=t-L+1}^{t}\boldsymbol{u}(t-i)\lambda_i\kappa_{\sigma ij}\boldsymbol{e}_p(t-j)\\ \Omega_3=\dfrac{1}{L^2\sigma^2}\displaystyle\sum_{i=t-L+1}^{t}\sum_{j=t-L+1}^{t}\boldsymbol{u}(t-j)\lambda_j\kappa_{\sigma ij}\boldsymbol{e}_p(t-i)\\ \Omega_4=\dfrac{1}{L^2\sigma^2}\displaystyle\sum_{i=t-L+1}^{t}\sum_{j=t-L+1}^{t}\boldsymbol{u}(t-j)\lambda_j\kappa_{\sigma ij}\boldsymbol{e}_p(t-j)\end{cases} \tag{18}$$

During this derivation, the kernel matrices $\boldsymbol{B}(t)$ and $\boldsymbol{A}(t)$, constructed from weighted errors, play pivotal roles throughout the optimization process. They are defined as

$$\boldsymbol{A}_{i,j}=\kappa_\sigma(\lambda_i\boldsymbol{e}_p(t-i)-\lambda_j\boldsymbol{e}_p(t-j)) \tag{19}$$

$$\boldsymbol{B}_{i,j}=\begin{cases}\displaystyle\sum_{i=1}^{L}\sum_{j=1}^{L}\boldsymbol{A}_{i,j} & i=j\\ 0 & i\neq j\end{cases} \tag{20}$$

Let $\boldsymbol{W}=\mathrm{diag}(\lambda_1,\lambda_2,\cdots,\lambda_L)$ is a diagonal weight matrix. Meanwhile, $\boldsymbol{E}_p(t)$ denotes the weighted error vector, formulated as

$$\boldsymbol{E}_p(t)=[\lambda_1\boldsymbol{e}_p(t-1),\lambda_2\boldsymbol{e}_p(t-2),\cdots,\lambda_L\boldsymbol{e}_p(t-L)]=\boldsymbol{W}[\boldsymbol{e}_p(t-1),\boldsymbol{e}_p(t-2),\cdots,\boldsymbol{e}_p(t-L)] \tag{21}$$

$\boldsymbol{X}(t)$ represents the weighted input signal matrix, expressed as

$$\boldsymbol{X}(t)=[\lambda_1\boldsymbol{u}(t-1),\lambda_2\boldsymbol{u}(t-2),\cdots,\lambda_L\boldsymbol{u}(t-L)]=\boldsymbol{U}(t)\boldsymbol{W}^{\mathrm{T}} \tag{22}$$

where $\boldsymbol{U}(t)=[\boldsymbol{u}(t-1),\boldsymbol{u}(t-2),\cdots,\boldsymbol{u}(t-L)]$ is the unweighted input matrix.

Setting Eq.(16) to zero yields the difference expression for consecutive weight vectors

$$\boldsymbol{w}(t)-\boldsymbol{w}(t-1)=\frac{1}{L^2\sigma^2\gamma}\boldsymbol{X}(t)(\boldsymbol{B}(t)-\boldsymbol{A}(t))\boldsymbol{E}_p(t) \tag{23}$$

To rigorously derive the Lagrange multiplier γ while ensuring optimization validity and reliability under complex conditions, we impose the strictest constraint $\|\boldsymbol{w}(t)-\boldsymbol{w}(t-1)\|_2^2=\mu^2$. Substituting Eq.(23) into this constraint and through rigorous mathematical derivation, we obtain

$$\gamma=\frac{1}{L^2\sigma^2\mu}\|\boldsymbol{X}(t)(\boldsymbol{B}(t)-\boldsymbol{A}(t))\boldsymbol{E}_p(t)\|_2 \tag{24}$$

Finally, substituting Eq.(24) into Eq.(23) yields the iterative update formula for weight vector $\boldsymbol{w}(t)$

$$\boldsymbol{w}(t)=\boldsymbol{w}(t-1)+\mu\frac{\boldsymbol{X}(t)(\boldsymbol{B}(t)-\boldsymbol{A}(t))\boldsymbol{E}_p(t)}{\|\boldsymbol{X}(t)(\boldsymbol{B}(t)-\boldsymbol{A}(t))\boldsymbol{E}_p(t)\|_2} \tag{25}$$

Eq.(25) explicitly defines the weight vector update mechanism at each iteration, serving as the computational cornerstone for the optimization algorithm based on affine projection spaces and the MMEE criterion. In practical applications, iterative execution of this formula enables real-time weight vector adaptation to varying signal environments based on input signals and error feedback.

3 Analysis of Stability

Before proceeding with the analysis, it is necessary to introduce the following assumptions, which are commonly adopted in the adaptive filtering.

Assumption 1 In practical applications, both $\boldsymbol{u}(t)$ and noise signal $\boldsymbol{v}(t)$ are considered as stationary random variables with zero mean.

Assumption 2 The auto correlation matrix of the input signal satisfies

$$E[\boldsymbol{u}(t)\boldsymbol{u}^{\mathrm{T}}(t)]=\sigma_u^2\boldsymbol{I} \tag{26}$$

It indicates that the input signals are mutually independent across different dimensions, with each dimension having identical variance σ_u^2.

Assumption 3 The auto correlation matrix of the noise satisfies

$$E[\boldsymbol{v}(t)\boldsymbol{v}^{\mathrm{T}}(t)]=\sigma_v^2\boldsymbol{I} \tag{27}$$

It implies that the noise components are also independent across dimensions with uniform variance σ_v^2.

Assumption 4 The noise signal $\boldsymbol{v}(t)$ is uncorrelated with the input vector sequence $\boldsymbol{x}(t)$. They are statistically independent, satisfying

$$E[\boldsymbol{u}(t)\boldsymbol{v}(t)]=0 \tag{28}$$

Assumption 5 The M-estimation weight function $\lambda_i=\varphi(\boldsymbol{e}_i)$, as the core element for achieving robustness in the APMMEE algorithm, is bounded within $\lambda_i\in[0,1]$. This constraint ensures that the weighting effect on error samples remains within a reasonable range, preventing excessive amplification or attenuation of error impacts.

To analyze the temporal evolution of the weight error vector $\tilde{\boldsymbol{w}}(t)$, we substitute the weight

update formula into $\tilde{\boldsymbol{w}}(t+1)=\boldsymbol{w}_0-\boldsymbol{w}(t+1)$, yielding

$$\tilde{\boldsymbol{w}}(t+1)=\tilde{\boldsymbol{w}}(t)-\mu\boldsymbol{U}(t)\boldsymbol{H}(t)(\boldsymbol{d}(t)-\boldsymbol{U}^{\mathrm{T}}(t)\boldsymbol{w}(t)) \tag{29}$$

where $\boldsymbol{H}(t)=\dfrac{\boldsymbol{W}^{\mathrm{T}}(\boldsymbol{B}(t)-\boldsymbol{A}(t))\boldsymbol{W}}{\|\boldsymbol{X}(t)(\boldsymbol{B}(t)-\boldsymbol{A}(t))\boldsymbol{E}_p(t)\|_2}$. This difference equation characterizes the relationship between current and subsequent weight error vectors, whose dynamical properties determine algorithm convergence to optimal weights and form the cornerstone of subsequent stability analysis. Incorporating the system model $\boldsymbol{d}(t)=\boldsymbol{U}^{\mathrm{T}}(t)\boldsymbol{w}_0+\boldsymbol{v}(t)$, where $\boldsymbol{d}(t)$ denotes the desired signal, we derive

$$\tilde{\boldsymbol{w}}(t+1)=\tilde{\boldsymbol{w}}(t)-\mu\boldsymbol{U}(t)\boldsymbol{H}(t)\boldsymbol{U}^{\mathrm{T}}(t)\tilde{\boldsymbol{w}}(t)-\mu\boldsymbol{U}(t)\boldsymbol{H}(t)\boldsymbol{v}(t) \tag{30}$$

This expression establishes explicit connections among weight deviation dynamics, input signals, noise, and current weight deviations, laying the foundation for stability analysis via statistical properties. Taking expectations on both sides (with zero-mean noise) yields

$$E[\tilde{\boldsymbol{w}}(t+1)]=E[\tilde{\boldsymbol{w}}(t)]-\mu E[\boldsymbol{U}(t)\boldsymbol{H}(t)\boldsymbol{U}^{\mathrm{T}}(t)]E[\tilde{\boldsymbol{w}}(t)] \tag{31}$$

To facilitate the analysis, we perform orthogonal decomposition of $\boldsymbol{H}(t)$

$$\boldsymbol{H}(t)=\boldsymbol{Q}\boldsymbol{\Sigma}\boldsymbol{Q}^{\mathrm{T}} \tag{32}$$

where $\boldsymbol{Q}$ is an orthogonal matrix $\boldsymbol{Q}\boldsymbol{Q}^{\mathrm{T}}=\boldsymbol{I}$, and $\boldsymbol{\Sigma}=\mathrm{diag}(\xi_1,\xi_2,\cdots,\xi_L)$ the diagonal eigenvalue matrix with $\xi_1,\xi_2,\cdots,\xi_L$ representing the eigenvalues of $\boldsymbol{H}(t)$.

From Assumption 2, we obtain

$$E[\boldsymbol{U}(t)\boldsymbol{U}(t)^{\mathrm{T}}]=E\Big[[\boldsymbol{u}(t),\boldsymbol{u}(t-1),\cdots,\boldsymbol{u}(t-L+1)]\cdot[\boldsymbol{u}(t),\boldsymbol{u}(t-1),\cdots,\boldsymbol{u}(t-L+1)]^{\mathrm{T}}\Big]=L\sigma_u^2\boldsymbol{I} \tag{33}$$

Combining Eq.(33) with Eq.(31) gives

$$E[\tilde{\boldsymbol{w}}(t+1)]=E[\boldsymbol{D}(t)(\boldsymbol{I}-\mu\boldsymbol{\Sigma})\boldsymbol{D}^{\mathrm{T}}(t)]E[\tilde{\boldsymbol{w}}(t)] \tag{34}$$

where $\boldsymbol{D}(t)=\boldsymbol{U}(t)\boldsymbol{Q}$, satisfying $E[\boldsymbol{D}(t)\boldsymbol{D}^{\mathrm{T}}(t)]=\boldsymbol{I}$.

To guarantee the algorithm's convergence to optimal weights, where the expectation of the weight error vector asymptotically approaches zero, the following condition must hold $\|E[\boldsymbol{D}(t)(\boldsymbol{I}-\mu\boldsymbol{\Sigma})\boldsymbol{D}^{\mathrm{T}}(t)]\|<1$. Given that $\boldsymbol{D}(t)(\boldsymbol{I}-\mu\boldsymbol{\Sigma})\boldsymbol{D}^{\mathrm{T}}(t)$ is a symmetric matrix, its norm equals the absolute value of the maximum eigenvalue. For the diagonal matrix $\boldsymbol{I}-\mu\boldsymbol{\Sigma}$ with eigenvalues $1-\mu\xi_j$ ($j=1,2,\cdots,L$), this condition is equivalent to requiring the spectral radius of $\boldsymbol{I}-\mu\boldsymbol{\Sigma}$ to be less than unity

$$|1-\mu\xi_j|<1 \tag{35}$$

Consequently, the step size must satisfy

$$0<\mu<\frac{2}{\max_j\xi_j} \tag{36}$$

4 Simulation Results

The superior performance of the proposed APMMEE algorithm is validated through computer simulations, with evaluation conducted using the normalized mean square deviation (NMSD), defined as

$$\mathrm{NMSD}(t)=10\lg\left(\frac{\|\boldsymbol{w}(t)-\boldsymbol{w}_0(t)\|_2^2}{\|\boldsymbol{w}_0(t)\|_2^2}\right) \tag{37}$$

where $\boldsymbol{w}(t)$ denotes the weight vector of the filter at time t, $\boldsymbol{w}_0(t)$ the reference vector at time t, $\|\cdot\|_2^2$ the squared l_2 norm of the vector, and $\lg(\cdot)$ the base-10 logarithm operation that transforms linear-domain deviations to decibel (dB)-scale results.

In the simulation experiments, the steady-state error serves to quantify the minimum achievable error after prolonged system operation. Ideally, this error should asymptotically approach zero, with smaller computed values indicating closer approximation to this ideal condition. The convergence rate is measured by the time required for the algorithm to achieve stable convergence, while the tracking performance is primarily characterized by the system's recovery speed to a new steady state following abrupt changes in impulse response. All experimental data represent averaged results from 300 independent simulation trials to ensure the reliability and scientific validity.

4.1 System identification

In the system identification experiment, the input signal is generated by filtering zero-mean, unit-

variance Gaussian white noise through a first-order filter with a transfer function of $F(z)=1/(1-0.7z^{-1})$. This experimental setup is designed to endow the input signal with specific correlation and spectral characteristics, thereby better approximating real-world non-white noise scenarios encountered in practical applications. The simple structure of the first-order filter ensures the rationality of the input signal while reducing simulation complexity, which facilitates the analysis of the adaptive algorithm's convergence performance and identification effectiveness. To simulate realistic conditions, the noise with a signal-to-noise ratio (SNR) of 30 dB is added to the input signal. This SNR level represents a commonly adopted reference value in engineering practice, as it maintains adequate signal quality while effectively evaluating the algorithm performance.

The background noise $v(t)$ in the experiment follows an α-stable distribution. The parameters of the α-stable distribution are specified by the vector $\boldsymbol{V}_{\alpha\text{-SD}}=[\alpha,\beta,\gamma,\delta]$[31]. The characteristic exponent α takes values in (0, 2), determining the tail characteristics of the α-stable distribution. In probability distributions, the tail corresponds to the probability of extreme outliers. As α decreases from 2, the tail of the α-stable distribution becomes heavier, indicating a significantly increased probability of outliers. To simulate anomalous outliers in the signal, the parameters of the α-stable distribution are set to [0.2, 0, 1.5, 0] for all system identification simulations.

Typically, the threshold parameters of Hampel's weight function are empirically determined, with common settings such as $\Delta_1=1.31$, $\Delta_2=2.039$, $\Delta_3=4$, or alternatively $\Delta_1=2$, $\Delta_2=4$, $\Delta_3=8$[32]. According to the literature on MMEE criterion[33], we select an optimal parameter set $\Delta_1=0.5$, $\Delta_2=2$, $\Delta_3=4$ to ensure peak performance of the proposed algorithm.

In the first experimental trial, we systematically investigate the performance of the APMMEE algorithm (step size $\mu=0.01$, filter length is 32) across varying kernel bandwidths $\sigma\in\{0.3, 0.5, 1.0, 2.0, 2.5\}$. As demonstrated by the experimental data in Fig.1, the kernel width $\sigma=1$ exhibits superior performance. In subsequent experiments, the kernel bandwidth is fixed at $\sigma=1$.

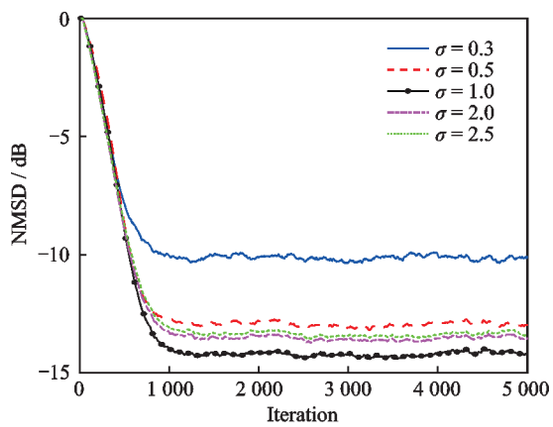

Fig.1 NMSD curves of the APMMEE algorithm versus parameter σ

The second experiment investigates the impact of varying projection orders $L\in\{8, 16, 32, 64\}$ on the performance of the APMMEE algorithm within the affine projection framework. As clearly illustrated in Fig.2, increasing the projection order leads to a significant improvement in the convergence rate of the APMMEE algorithm, albeit at the expense of a slight degradation in steady-state accuracy.

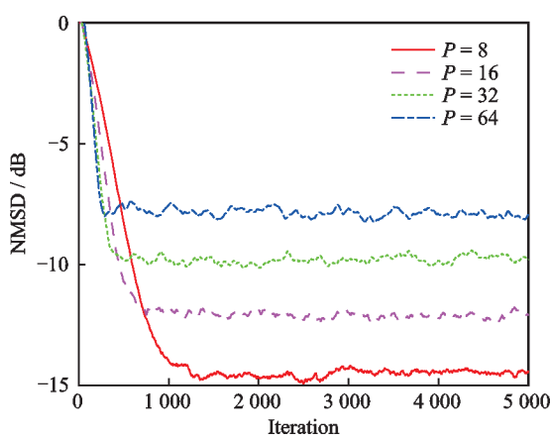

Fig.2 NMSD performance of APMMEE versus projection order

The third experiment comparatively evaluates the performance of LMS ($\mu=0.08$), AP ($\mu=0.074$), APSA[34] ($\mu=0.069$), APMEE ($\mu=0.008\ 5$), and the proposed APMMEE algorithm ($\mu=0.008\ 5$) under identical projection order ($P=$

32). As demonstrated in Fig.3, the APMMEE algorithm exhibits significant advantages in both convergence rate and steady-state accuracy.

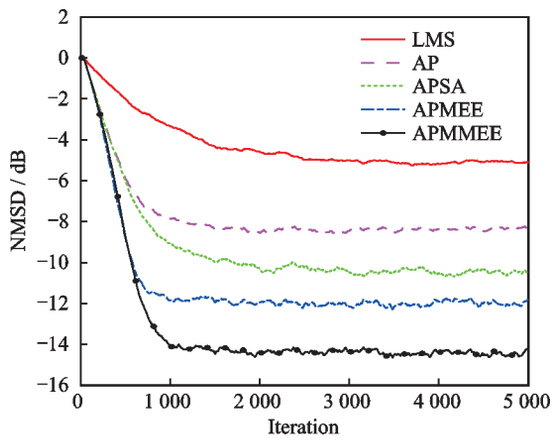

Fig.3 NMSD performance comparison of LMS, AP, APSA, APMEE and the proposed APMMEE under α-stable noise

In α-stable non-Gaussian noise environments, the LMS algorithm fails to distinguish between normal errors and outliers, resulting in sluggish convergence; while the AP algorithm accelerates convergence through block updates, its lack of targeted suppression mechanisms causes trajectory deviation from the optimal path and inability to reduce the steady-state error. The APSA algorithm demonstrates limited utilization of input correlations and restricted non-Gaussian noise handling capability. Although it achieves faster convergence and lower NMSD compared to LMS and AP, its inadequate exploitation of higher-order statistics results in weak noise suppression and higher steady-state error than both APMEE and APMMEE. The APMEE algorithm inherits the fast convergence characteristic of the AP algorithm's multi-data-block joint update mechanism, while demonstrating competent performance through the MEE criterion's flexible characterization of signal probability distributions. However, the APMEE lacks dedicated outlier suppression mechanisms, allowing anomalies to corrupt the error entropy calculation, which biases weight updates and induces convergence fluctuations or performance degradation. In contrast, the APMMEE preserves both the AP algorithm's rapid convergence and MEE's non-Gaussian noise adaptability, while incorporating an M-estimation weighting mechanism to establish dedicated outlier suppression. This design enables stable convergence under extreme outlier interference, with APMMEE outperforming APMEE and LMS in both the convergence speed across all scenarios and achieving optimal steady-state NMSD performance. Consequently, it delivers purer echo data for subsequent spaceborne SAR imaging processing.

The fourth experiment compares the performance of the proposed APMMEE algorithm (μ = 0.008 7) with APSA (μ =0.075), LMS (μ = 0.095), AP (μ =0.081), and APMEE (μ = 0.008 8) under varying sparse system conditions. The experiment is configured with 3×10^4 iterations, where the unknown system coefficients are regenerated at the 10 000th and 20 000th iterations to simulate parameter abrupt changes, respectively. The filter length is set to 32, initialized as a unimodal sparse system (only the 9th element = 1), transformed to bimodal after the first abrupt change (5th=1, 32nd=−1), and then to trimodal after the second abrupt change (1st, 32nd=1, 16th=−1). As shown in Fig.4, the proposed algorithm demonstrates superior adaptability to environmental abrupt changes and maintains excellent steady-state error control across different sparse systems. Its robustness provides strong support for stable operation in complex dynamic environments and heterogeneous systems.

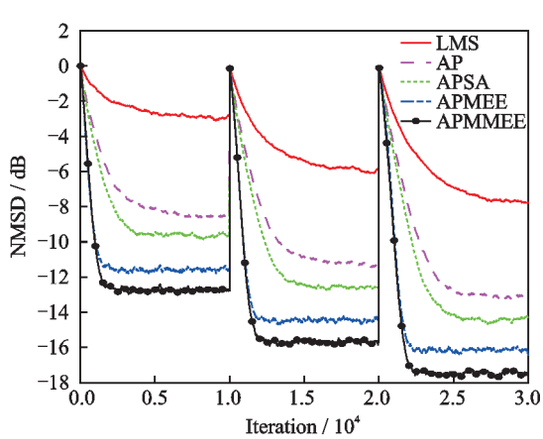

Fig.4 Comparative analysis of NMSD performance for five algorithms under abrupt sparse structure transitions (unimodal → bimodal → trimodal)

4.2 Real-signal multipath interference cancellation

As an active microwave remote sensing system, spaceborne SAR typically employs LFM signals to achieve pulse compression through frequency modulation, thereby enhancing the range resolution while maintaining operational range. During the signal propagation to the target area and reflection back to the sensor, multipath interference occurs due to multiple propagation paths, such as when encountering discontinuous structures where signal diffraction creates additional paths, or when mountainous terrain causes multiple reflections, generating multipath components with different propagation distances and phases compared to the direct path. These redundant multipath interference components, which corrupt the genuine information we receive, are combined with environmental additive noise to form composite signals containing both useless information from multipath interference and random noise disturbances. The resulting high complexity poses significant challenges for subsequent signal processing and target detection.

The fifth experiment evaluating multipath interference suppression performance systematically compares the proposed APMMEE algorithm ($\mu=0.005$) with LMS ($\mu=0.4$), AP ($\mu=0.09$), APSA ($\mu=0.08$), and APMEE ($\mu=0.09$) algorithms under varying outlier interference intensities, comprehensively validating their robustness in suppressing SAR multipath interference within complex noise environments. The filter tap length is configured as $M=128$, sufficiently covering typical multipath delay ranges (e.g., 50—200 ns) in spaceborne SAR echoes to ensure effective processing of redundant multipath components at varying distances. Fig.5(a) displays waveform characteristics of actual spaceborne SAR raw echoes contaminated by 30 dB SNR Gaussian noise, establishing the baseline interference scenario under clear-sky conditions. Two characteristic α-stable noise scenarios are designed to accurately match complex spaceborne SAR observation environments. Fig.5(b) shows Scenario Ⅰ with parameters [1.2, 0, 1, 0] (characteristic exponent $\alpha=1.2$), exhibiting relatively light-tailed characteristics where the probability density function decays rapidly with lower outlier occurrence frequency. This corresponds to suburban environments where sparse low-rise buildings and vegetation generate weaker redundant multipath interference, representing moderate non-Gaussian interference. Fig.5(c) presents Scenario Ⅱ with parameters [0.3, 0, 1, 0] ($\alpha=0.3$), demonstrating heavy-tailed characteristics with slower probability density function decay and significantly increased outlier probability. This simulates dense urban areas or stormy weather where numerous high-rise reflections and atmospheric scattering create strong redundant multipath with frequent outliers, rigorously testing algorithm performance under extreme non-Gaussian noise conditions.

Fig.5(b) demonstrates that while conventional algorithms achieve basic suppression of redundant multipath interference in spaceborne SAR echoes, their performance diverges due to inadequate adaptation mechanisms to complex SAR noise statistics. In suburban moderate-interference scenarios, they show insufficient suppression precision for multipath components with delays close to the direct signal, manifesting as larger error fluctuations and slower convergence rates that fail to meet subsequent imaging requirements for echo purity. These deficiencies are exacerbated in the high-outlier scenario of Fig.5(c). Strong redundant multipath interference in dense urban/inclement weather conditions generates numerous extreme values, causing conventional algorithms to frequently deviate from optimal weight trajectories, worsening steady-state errors and inducing persistent convergence oscillations. This impairs their ability to discriminate between true target scattering signals and interference components, significantly degrading the SAR imaging resolution and edge sharpness. In contrast, the APMMEE algorithm outperforms in both scenarios through its integrated M-estimation weighting mechanism that dynamically identifies multipath-induced outliers in SAR echoes. It assigns low weights to large-magnitude interference while maintaining high sensitivity to valid direct-path components, ensuring stable

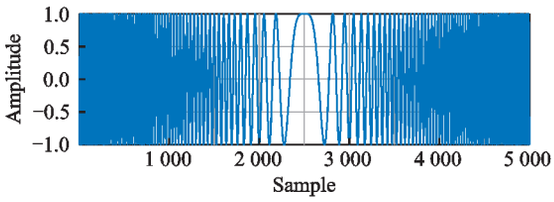

(a) Input signal waveforms in multipath interference suppression experiments

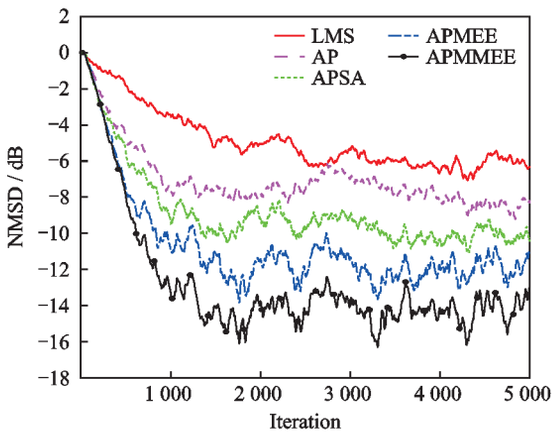

(b) NMSD performance of five algorithms for multipath interference suppression under α-stable noise with parameters [1.2, 0, 1, 0]

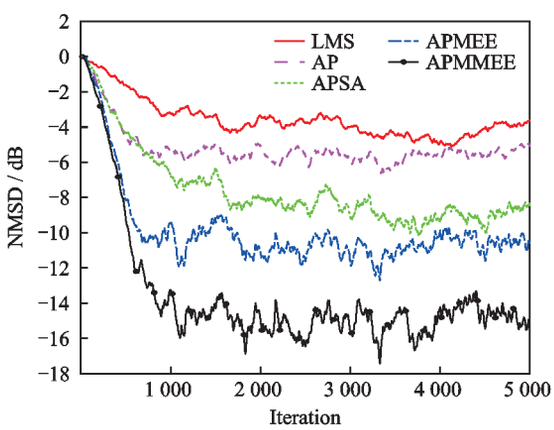

(c) NMSD performance of five algorithms for multipath interference suppression under α-stable noise with parameters [0.3, 0, 1, 0]

Fig.5 Wave diagrams of the input signal and performance comparison of the algorithm under different levels of noise in a stationary enviroment

convergence even under severe outlier interference. These results conclusively demonstrate APMMEE's superior redundant multipath suppression capability in spaceborne heavy-tailed clutter environments, and providing more reliable signal purification for spaceborne SAR raw echo preprocessing, thereby advancing practical applications of SAR redundant multipath interference suppression in complex scenarios.

In the sixth experiment addressing redundant multipath interference suppression for spaceborne SAR under high-dynamic observation scenarios, the investigation is conducted under [0.7, 0, 1, 0] noise conditions, where these noise parameters simulate complex environments with random variations in multipath delays and amplitudes caused by rapid radar beam scanning across undulating mountainous terrain, with redundant multipath interference primarily arising from combined mountain reflections and surface scattering. To accurately emulate high-dynamic channel characteristics of spaceborne SAR (where satellite high-speed motion causes abrupt changes in beam illumination areas leading to drastic multipath propagation variations), a channel mutation is introduced at the 2 500th iteration by implementing both channel inversion processing and switching to random sparse configurations, with corresponding experimental results presented in Figs.6 (a) and 6(b).

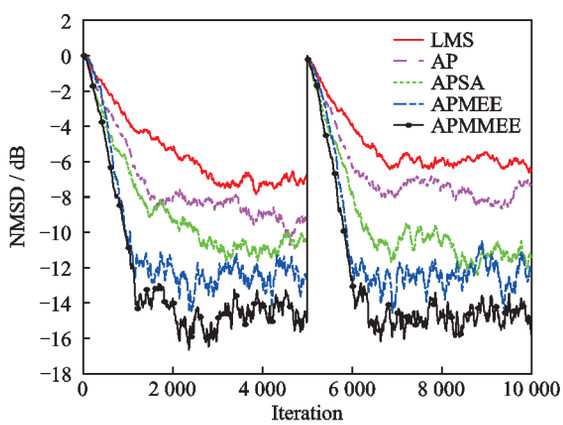

(a) NMSD performance of five algorithms for multipath interference suppression under channel inversion mutation

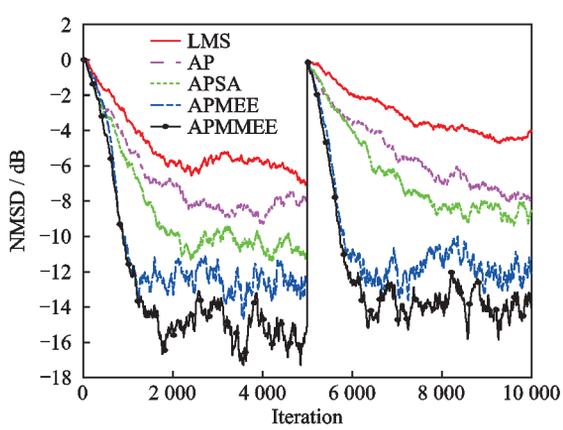

(b) NMSD performance of five algorithms for multipath interference suppression under random sparse channel mutation

Fig.6 Performance comparison of the algorithm under different levels of noise in a non-stationary environment

Fig.6(a) clearly demonstrates that conventional algorithms exhibit significant tracking lag when channel mutations occur in spaceborne SAR systems. Their weight-updating mechanisms fail to promptly adapt to rapid multipath interference variations, causing notable fluctuations in suppression performance, sudden drops in target echo SNR, and direct degradation of phase coherence in subsequent imaging. These limitations become more pronounced in the random sparse channel scenario depicted in Fig.6(b). The random sparse channel emulates the stochastic appearance/disappearance of multipath sources when beams scan steep terrains. In these steep terrains, the impulsive and non-stationary characteristics amplify error signal anomalies, substantially reducing conventional algorithms' convergence speed, increasing the steady-state error, and consequently impairing multipath interference suppression capability. In contrast, the proposed APMMEE algorithm achieves rapid parameter adaptation, dynamically filtering strong multipath outliers during mutations through its M-estimation weighting mechanism, while simultaneously tracking channel variations via multi-data-block joint updates to maintain stable convergence speed and low steady-state error. It outperforms comparative algorithms in both post-mutation recovery capability and tracking precision, enabling accurate redundant multipath suppression in dynamic scenarios, conclusively validating its superior performance in complex non-stationary spaceborne SAR observation environments.

5 Conclusions

In the context of multipath interference suppression and outlier processing in spaceborne SAR, this paper proposes the M-estimation-based minimum error entropy with affine projection algorithm. Its dedicated framework addresses redundant multipath interference from building diffraction and terrain reflection by assigning differential weights to urban and mountainous scattering outliers via a weighting function, dynamically optimizing the error vector, and imposing a l_2-norm constraint to enhance adaptability in complex environments. Simulation results demonstrate that the proposed algorithm exhibits excellent multipath tracking capability in sparse systems simulating urban clusters and undulating terrains, effectively capturing delay and amplitude variations. In heavy-tailed interference environments such as strong urban reflections and storm pulses, it can achieve faster convergence and lower steady-state error than conventional methods, and mitigate the convergence instability and accuracy degradation caused by outliers, thereby providing more reliable suppression for SAR raw echo preprocessing. However, when processing ultra-large-scale data such as full-aperture imaging, joint updates of multiple data blocks increase the memory overhead. Future work will focus on lightweight architectures, leveraging the range-azimuth separability of SAR echoes to optimize data partitioning and parallel processing, thereby supporting higher-precision spaceborne SAR imaging and multipath suppression.

References

[1] JIA P, DONG T C, WANG T Y, et al. Dual-domain joint dense multiple small ship target detection algorithm for spaceborne SAR images[J]. Transactions of Nanjing University of Aeronautics and Astronautics, 2024, 41(6): 725-738.

[2] CAO Z, LI P, TANG W, et al. Self-position determination based on array signal subspace fitting under multipath environments[J]. Sensors, 2023, 23(23): 9356.

[3] SUZUKI K, YUKAWA M. Sparse stable outlier-robust signal recovery under Gaussian noise[J]. IEEE Transactions on Signal Processing, 2023, 71: 372-387.

[4] LIAO M, CUI G, XIONG K, et al. Variable false alarm rate detection framework for phased array radar[J]. IEEE Transactions on Aerospace and Electronic Systems, 2023, 59(5): 6314-6326.

[5] MA C Y. Analysis on beamforming of whole airspace phased array TTC system based on linear subarrays[J]. Transactions of Nanjing University of Aeronautics and Astronautics, 2015, 32(1): 128-132.

[6] PATNAIK A, NANDA S. A switching norm based least mean square/fourth adaptive technique for sparse channel estimation and echo cancellation[J]. Physical Communication, 2024, 67: 102482.

[7] MOINUDDIN M, ZERGUINE A, ARIF M. A weighted Gaussian kernel least mean square algorithm[J]. Circuits, Systems, and Signal Processing, 2023, 42(9): 5267-5288.

[8] SUN K P, HU H Y, ZHAO Y H. Identification of time-varying modal parameters for thermo-elastic structure subject to unsteady heating[J]. Transactions of Nanjing University of Aeronautics and Astronautics, 2014, 31(1): 39-48.

[9] FÎCIU I D, STANCIU C L, ELISEI-ILIESCU C, et al. Tensor-based recursive least-squares adaptive algorithms with low-complexity and high robustness features[J]. Electronics, 2022, 11(2): 237.

[10] BEKRANI M, ZAYYANI H, MOHAGHEGHIAN-BIDGOLI Z. Improved affine projection algorithms with selective projection order for channel identification[J]. Signal, Image and Video Processing, 2024, 18(12): 8645-8657.

[11] ZHOU X, LI G, WANG Z, et al. Robust hybrid affine projection filtering algorithm under α-stable environment[J]. Signal Processing, 2023, 208: 108981.

[12] LU Y H, ZHANG J, LI X Y, et al. A robust method for adaptive center extraction of linear structured light stripe[J]. Transactions of Nanjing University of Aeronautics and Astronautics, 2020, 37(4): 586-596.

[13] LI Y, ZHOU J, TIAN J, et al. Weighted error entropy-based information theoretic learning for robust subspace representation[J]. IEEE Transactions on Neural Networks and Learning Systems, 2021, 33(9): 4228-4242.

[14] MITRA R, KADDOUM G, DAHMAN G, et al. Error analysis of localization based on minimum-error entropy with fiducial points[J]. IEEE Communications Letters, 2020, 25(4): 1187-1191.

[15] WANG G, YANG X, WU L, et al. A kernel recursive minimum error entropy adaptive filter[J]. Signal Processing, 2022, 193: 108410.

[16] WANG X, OU S, GAO Y. Convex regularized recursive minimum error entropy algorithm[J]. Electronics, 2024, 13(5): 992.

[17] ZHANG H, LI G, HOU Y, et al. Minimum error entropy with affine projection algorithm for robust adaptive filtering[J]. Digital Signal Processing, 2025, 163: 105198.

[18] MURALISHANKAR R, GHOSH D, GURUGOPINATH S. Robust voice activity detection based on weighted average of long-term quadratic Renyi and differential entropies[J]. Digital Signal Processing, 2022, 131: 103756.

[19] ZHONG S, PENG B, WANG Z, et al. Outlier-aware recursive instantaneous minimum error entropy algorithm[J]. IEEE Transactions on Systems, Man, and Cybernetics: Systems, 2025, 55(6): 4076-4090.

[20] WU S D, SHANG D G, SHI F T, et al. A probability density function of stress amplitude applicable to power spectral density curves of structural random vibration response[J]. International Journal of Fatigue, 2024, 186: 108408.

[21] FU H, CHENG Y. Switching Gaussian-heavy-tailed distribution based robust Gaussian approximate filter for INS/GNSS integration[J]. Journal of the Franklin Institute, 2022, 359(16): 9271-9295.

[22] YANG D, KUANG H, YANG K, et al. Towards asynchronous multimodal signal interaction and fusion via tailored transformers[J]. IEEE Signal Processing Letters, 2024, 31: 1550-1554.

[23] ZHONG S, WANG Z, WANG G, et al. Robust adaptive filtering based on M-estimation-based minimum error entropy criterion[J]. Information Sciences, 2024, 658: 120026.

[24] CHEN X, SHENG W. Robust adaptive beamforming via quasi-signal subspace estimation for covariance matrix reconstruction[J]. Digital Signal Processing, 2024, 150: 104531.

[25] ZHOU Z, HUANG L, CHRISTENSEN M G, et al. Robust spectral analysis of multi-channel sinusoidal signals in impulsive noise environments[J]. IEEE Transactions on Signal Processing, 2021, 70: 919-935.

[26] WU Q, LI Y, ZAKHAROV Y V, et al. A kernel affine projection-like algorithm in reproducing kernel hilbert space[J]. IEEE Transactions on Circuits and Systems Ⅱ: Express Briefs, 2019, 67(10): 2249-2253.

[27] GUO J, KEPLER M E, TEJ PARUCHURI S, et al. Adaptive estimation of external fields in reproducing kernel Hilbert spaces[J]. International Journal of Adaptive Control and Signal Processing, 2022, 36(8): 1931-1957.

[28] HU M H, ZHANG X, YUAN L G, et al. Identifying similar operation scenes for busy area sector dynamic management[J]. Transactions of Nanjing University of Aeronautics and Astronautics, 2020, 37(4): 615-629.

[29] ZHAI Y, YANG J, ZHANG S, et al. Linear frequency modulated signal induced aperiodic resonance[J]. Physica Scripta, 2020, 95(6): 065213.

[30] LU Z, GAO M, LI Y, et al. Performance analysis of direct signal and surface clutter cancellation for bistatic

noise radar with LMS filter[C]//Proceedings of IEEE 10th International Conference on Industrial Informatics. [S.l.]: IEEE, 2012: 184-189.

[31] SHAO M, NIKIAS C L. Signal processing with fractional lower order moments: Stable processes and their applications[J]. Proceedings of the IEEE, 2002, 81(7): 986-1010.

[32] WANG H, LI H, ZHANG W, et al. A unified framework for M-estimation based robust Kalman smoothing[J]. Signal Processing, 2019, 158: 61-65.

[33] ZHONG S, WANG Z, WANG G, et al. Robust adaptive filtering based on M-estimation-based minimum error entropy criterion[J]. Information Sciences, 2024, 658: 120026.

[34] SHAO T, ZHENG Y R, BENESTY J. An affine projection sign algorithm robust against impulsive interferences[J]. IEEE Signal Processing Letters, 2010, 17(4): 327-330.

Acknowledgement This work was supported by Shandong Provincial Natural Science Foundation (No.ZR2022MF314).

Authors

The first author Mr. **WANG Weixin** received his B.S. degree in electronic information science and technology from School of Physics and Electronic Information, Yantai University in 2024. Since 2024, he has been pursuing his M.S. degree in electronic science and technology at Yantai University. His research interest focuses on intelligent signal processing.

The corresponding author Prof. **OU Shifeng** received the B.S. degree in electronic information engineering in 2002 and the M.S. degree in signal and information processing in 2005, both from College of Communication Engineering, Jilin University, Changchun, China. He obtained the Ph.D. degree in communication and information systems from the same university in 2008. Since 2008, he has been with School of Physics and Electronic Information, Yantai University, Yantai, China, where he is currently a Professor and Master's Supervisor. His current research interests include intelligent speech signal processing and blind signal processing.

Author contributions Mr. **WANG Weixin** led the research design, developed the algorithm, designed and analyzed system identification simulations, and wrote key manuscript sections. Ms. **CHANG Xuelian** contributed to establishing algorithm evaluation metrics, organized experimental data, and assisted in practical interference suppression experiments. Prof. **OU Shifeng** analyzed performance limitations of conventional adaptive filtering algorithms in SAR systems, participated in research discussions and background section writing, and provided critical revisions to the manuscript's logical structure. All authors commented on the manuscript draft and approved the submission.

Competing interests The authors declare no competing interests.

(Production Editor: WANG Jing)

基于M估计的最小误差熵仿射投影算法在星载SAR系统离群值抑制中的应用

王伟鑫，常雪莲，欧世峰

（烟台大学物理与电子信息学院，烟台 264005，中国）

摘要：传统自适应滤波算法在处理星载合成孔径雷达系统原始回波中的多径干扰时，常因异常离群值导致性能退化，表现为收敛不足与估计精度低下。针对该问题，本文提出一种新型鲁棒自适应滤波算法——基于M估计的最小误差熵仿射投影算法。该算法继承仿射投影算法的多数据块联合更新机制，能够快速适配原始回波的动态特性，实现快速收敛；同时融入基于M估计的最小误差熵准则，通过M估计函数对原始回波中的误差样本进行加权处理，在算法更新过程中有效抑制离群值干扰。系统辨识仿真与基于原始回波的实际多径干扰抑制实验均表明，所提算法具有更优异的滤波性能。

关键词：雷达信号；自适应滤波；最小误差熵；M估计；仿射投影